Physica B 642 (2022) 414128

Contents lists available at ScienceDirect

Physica B: Physics of Condensed Matter

journal homepage: www.elsevier.com/locate/physb

Spin state bistability in (Mn, Zn) doped $Fe(phen)_2(NCS)_2$ molecular thin film nanocrystals on quartz

Saroj Saha, Paramesh Chandra, Swapan K. Mandal *

Department of Physics, Visva-Bharati, Santiniketan, 731 235, India

ARTICLE INFO

Keywords:
Spin crossover
Spin state bistability
Magnetization
Thermal hysteresis
Transition temperature

ABSTRACT

Spin state bistability within high spin (HS) and low spin (LS) state is investigated in undoped and (Zn, Mn) doped spin crossover (SCO) complex $Fe(phen)_2(NCS)_2$ thin films (thickness ~ 300 nm) deposited by dip-coating technique at room temperature on the quartz substrate. The X-ray diffraction studies clearly show the formation of crystalline structure of SCO complexes. The growth of the thin films was indisputably confirmed by electron microscopy and optical studies. The optical absorption peak between 535-557 nm was clearly observed, and that corresponds to $^1A_{1g} \rightarrow {}^1T_{1g}$ ligand field absorption in undoped and metal-doped (Zn, Mn) SCO thin films. The high spin (HS) state of the SCO films at room temperature was confirmed by Raman spectra. The bistability of spin states is clearly revealed by the well pronounced thermal hysteresis loop in magnetization measurements. The spin transition temperature ($T_{1/2}$) and loop width are found to be critically dependent on metal doping and suggested the possibility of tuning these parameters in spin-crossover thin films to design future spin-based devices.

1. Introduction

The spin crossover (SCO) materials capable of spin-state switching are currently an important topic in material science research. The elements that have electronic configurations between $3d^4$-$3d^7$ may reveal the SCO phenomenon [1–5]. The electron distribution between lower energy (d_{xy}, d_{xz}, d_{yz}) to higher energy (d^2_{x-y}, d^2_z) state or vice versa in the d-orbital octahedral environment leads to the spin crossover phenomena. This spin crossover for the molecular complexes are governed by the interplay between crystal field splitting (Δ) and electronic pairing energy (p). When these two are nearly equal (Δ≈p), it can be overcome with a controllable and reversible various physical (*e.g.* temperature, pressure, electromagnetic irradiation) [6–12] or chemical stimuli [13–18]. The lower and higher energy state is called t_{2g} and e_g, respectively [19,20]. The materials that show the SCO property has become very popular for the use of various purposes such as memory devices, display, switching, refrigerant *etc.* [1,21–24]. Doping is widely used to modify nanoparticles to enhance their electrical, optical, magnetic, and biological activities [25–31]. The various dopant impurities also play an essential role in SCO complexes altering the host complexes' electronic structure and modulations. It is observed that doping in SCO complexes may tune the transition temperature ($T_{1/2}$) of SCO complexes [13–18]. In this investigation, $Fe(phen)_2(NCS)_2$ has been used as SCO material [2–5,18,19], and Zn, Mn has been used as equivalent dopant metals [14,15]. The materials used for making thin films play a unique role in developing smart devices for modern technologies [31–38]. The quartz is used here as a substrate by virtue of its clear optical transparency, dimensional stability, exalted hardness, and high-quality surface smoothness [15,38]. We have earlier studied the effect of metal dilution in SCO thin film on a glass substrate [15]. In this report, we have investigated whether any significant changes take place in Fe $(phen)_2(NCS)_2$ thin film due to the different substrate (quartz) and metal dilution strength (Mn, Zn). This kind of structural properties may affect the effective cooperativity between the molecules and therefore, in spin-state switching of the SCO complexes that was revealed in magnetization studies reported here. The most two important parameters are the hysteresis loop (and the loop width) in the magnetization curves and the spin transition temperature. For thermal stability of the devices, the loop widths are to be large enough so that a minute thermal fluctuation don't affect the device operations. On the other hand, devices operating at room temperature is quite essential for practical purposes [39]. Therefore, manipulating theses parameters, particularly in thin film structures, are crucial for spin crossover materials for smart devices. We report here and discuss on these issues in metal diluted Fe

* Corresponding author.
E-mail address: sk_mandal@hotmail.com (S.K. Mandal).

https://doi.org/10.1016/j.physb.2022.414128
Received 17 February 2022; Received in revised form 6 June 2022; Accepted 19 June 2022
Available online 28 June 2022

$(phen)_2(NCS)_2$ thin films.

2. Experiment details

Chemicals used for the synthesis of undoped (pure) $Fe(phen)_2(NCS)_2$ SCO material are 1,10-phenanthroline [$C_{12}H_8N_2$], Mohr's Salt [$(NH_4)_2Fe(SO_4)_2{\cdot}6H_2O$], Sodium thiocyanate [NaSCN]. The reagent used for the preparation of doping $Fe(phen)_2(NCS)_2$ are zinc chloride [$ZnCl_2$] and manganese chloride tetrahydrate [$MnCl_2{\cdot}4H_20$] for Zn and Mn doping, respectively. All the given chemicals have been taken with genuine analytical grade and used without further purification. The thin films of doped and undoped spin-crossover materials $Fe(phen)_2(NCS)_2$, $Fe_{1-x}Zn_x(phen)_2(NCS)_2$, and $Fe_{1-x}Mn_x(phen)_2(NCS)_2$ [x = (0,15,30)%] are deposited on quartz substrates with using a dip-coater, which is developed in our laboratory, and rate of deposition was kept 0.1 mm/s. The undoped and doped SCO complexes' have been synthesized by a normal wet-chemical process [15,37,38]. The quartz substrates are cleaned up properly and were further sonicated for 20 min with water, acetone medium for 10 min, and then 10 min with 2-propanol. The undoped $Fe(phen)_2(NCS)_2$ and doped $Fe_{1-x}Zn_x(phen)_2(NCS)_2$, and $Fe_{1-x}Mn_x(phen)_2(NCS)_2$ [x = 0%, 15%, 30%] complexes were synthesized using a procedure in a similar way to the previous study on SCO thin film on glass [15]. At first, the calculated amount (molar ratio) of the phenanthroline (organic compound) and Mohr's Salt were separately dissolved with distilled water. They were constantly stirred well for half an hour. Mohr's Salt solutions were then mixed in the phenanthroline solution properly, resulting in a deep red solution instantly. In the next step, the saturated NaNCS solution was added to the red solution and formed a complex salt $[Fe(phen)_3](NCS)_2$ and sonicated for 20 min [40,41]. Afterward, thin films of compound $[Fe(phen)_3](NCS)_2$ were fabricated on clean and transparent regular shaped quartz substrates with a dip-coater using distilled water as a solvent. During the preparation of metal-doped SCO complexes, a calculated amount of chemicals $MnCl_2{\cdot}4H_20$ (for Mn-doped) or $ZnCl_2$ (for Zn-doped) was mixed well into the prepared $Fe(phen)_3(NCS)_2$ red solution and stirred well for 20 min. Thin films of doped complexes $[Fe_{1-x}Mn_x(phen)_3](NCS)_2$, and $[Fe_{1-x}Zn_x(phen)_3](NCS)_2$ [x = (0,15,30)%] were then obtained using the dip-coating method. All the thin films were annealed at 190 °C in a vacuum ($\sim 10^{-3}$ Torr) for 1 h to obtain $[Fe(phen)_3](NCS)_2$ to $Fe(phen)_2(NCS)_2$. We observed a change in colour of the samples from red to violet. Finally, we have obtained the desired thin film of undoped $Fe(phen)_2(NCS)_2$, and doped $Fe_{1-x}Mn_x(phen)_2(NCS)_2$ or $Fe_{1-x}Zn_x(phen)_2(NCS)_2$ spin-crossover thin films (~300 nm thick) on quartz substrates which were used for further characterizations.

The morphology of the doped and undoped SCO thin films was studied using the scanning electron microscope (SEM, Model: ZEISS GEMINI 450) operated at a 20 kV accelerating voltage. The crystallinity of the thin films was recorded in the range 10^0-50^0 (2θ) by powder x-ray diffraction (XRD) (with an accuracy 0.01^0) with using Cu-Kα radiation (model: Bruker D8 Advance XRD). Raman scattering experiments were carried out for all the thin film samples (model: Labram-HR, Jobin Yvon, accuracy of wavenumber ~ 1 cm^{-1}). The optical absorption measurement for all the thin film samples was performed on the UV–Vis spectrometer (model: Beckman Coulter DU-720, accuracy ±1 nm). The temperature dependent magnetic measurement was also carried out using a high-sensitive ($\leq 10^{-8}$ emu) SQUID magnetometer (Model: MPMS5S) at a constant magnetic field 1T for detailed investigations.

3. Results and discussions

The nanostructure of spin crossover thin films of undoped and (Zn or Mn) doped $Fe(phen)_2(NCS)_2$ on quartz surface are shown in Fig. 1(a–c). The sample morphology clearly shows the homogeneous self-assembled granular growth of $Fe(phen)_2(NCS)_2$ nanoparticles with a grain size ~10 nm. These nanoparticles have formed an excellent granular arrangement with dense growth in all cases. The nature of the substrate, adhesion of the molecules on the substrate, the surface tension of the precursor solution, and crystallinity of the substrate eventually control the growth of the homogeneous films. The morphology of the films didn't change upon metal doping.

The phase state, purity, and crystal structure of undoped and the metal-doped spin-crossover thin film of $Fe(phen)_2(NCS)_2$ have been studied by XRD as shown in Fig. 2(a–c). The prominent reflected peaks of XRD patterns in Fig. 2 established the crystalline growth of all complexes very similar to the host SCO material. However, a slight shift

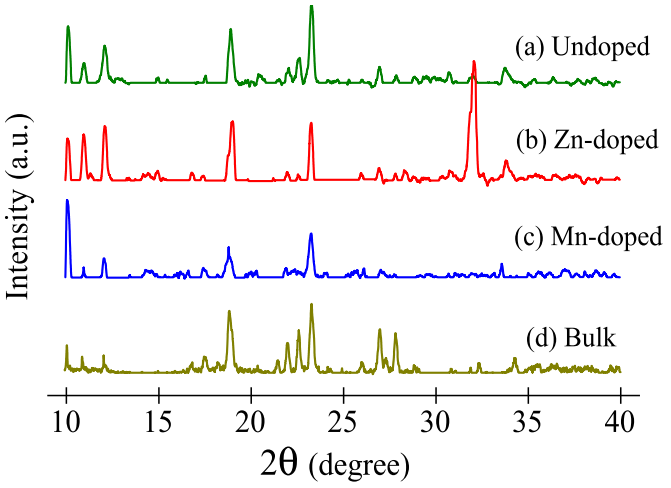

Fig. 2. Representative XRD pattern of spin-crossover thin films of (a) undoped, (b) Zn-doped (30%) (c) Mn-doped (30%) on quartz. The data has been compared with (d) bulk $Fe(phen)_2(NCS)_2$ at room temperature.

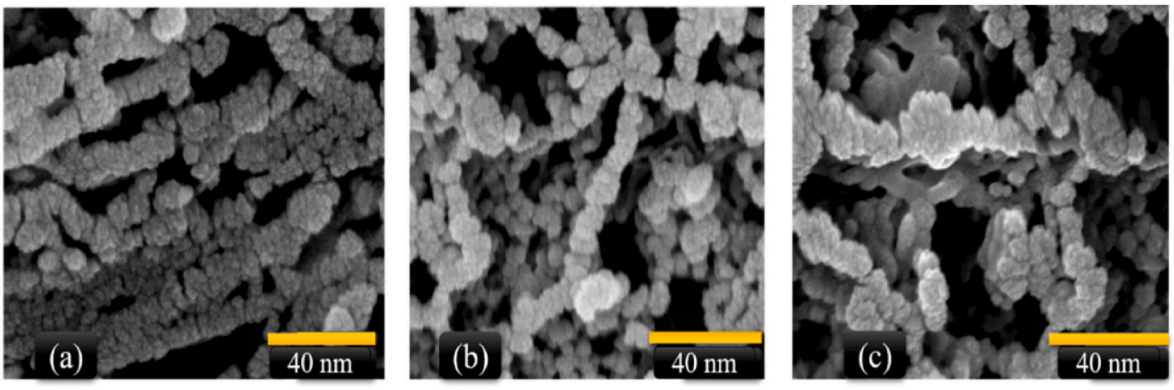

Fig. 1. Scanning electron microscope (SEM) images of (a) undoped, (b) Zn-doped and (c) Mn-doped SCO thin film of $Fe(phen)_2(NCS)_2$ on quartz.

(~0.1^0) in the lower angle peaks has been noticed for the doped samples. With respect to the undoped sample, the peaks are found to be blue-shifted for Mn-doped (30%) sample and that of red shifted for Zn-doped (30%) sample. The dopant ions substitute the Fe^{+2} ions in the lattice site and since the ionic radius of Mn^{+2} (81 pm) is slightly larger compared to Fe^{+2} (78 pm) and the ionic radius of Zn^{+2} (76 pm) is slightly smaller compared to host ions. So, the shift in the XRD peak position to lower and higher angle value may be ascribed to the lattice strain occurred in doped sample [42]. The nanoparticle's average size has been calculated using FWHM values of XRD peaks from the Scherrer equation, and it is found to be ~14 nm, which is quite similar to SEM data.

XRD data was further analysed with Rietveld refinement and lattice parameters thus obtained are summarized in Table 1. The data shows that the lattice parameters increased for Mn doped sample while for Zn doped sample the lattice parameters are found to decrease in comparison to the undoped sample. The results are consistent with the fact that Mn(II) has larger ionic radius than Fe(II) while the ionic radius of Zn(II) is smaller than that of Fe(II). So the change in lattice parameters in (Zn, Mn) doped SCO complexes may be attributed primarily to the ionic size effect and further confirms the doping [43].

The impression of different metal doping on the structure of the SCO thin film was also investigated using Raman spectroscopy. Raman scattering data of the synthesized undoped and also doped spin-crossover thin films is depicted in Fig. 3(a–c). As shown in Fig. 3a, the position of the peak of the SCO material $Fe(phen)_2(NCS)_2$ at 2065 cm^{-1} (SC–N symmetric stretching) exhibits the high spin (HS) nature characteristic at room temperature due to spin transition distribution [44–47]. This similar HS mode can also be found at 2063 cm^{-1}, and 2065 cm^{-1} for Zn(II) and Mn(II) diluted, as shown in Fig. 3b and c, respectively. The data confirms the similar molecular structure of the doped samples to that of the host compound due to the ionic radius of Zn (II) and Mn(II) comparable with HS Fe(II) at room temperature. For Mn doped sample, the peaks occurring at 85 cm^{-1} and 1586 cm^{-1} shifted significantly from that of undoped and Zn doped samples. This plausibly occurred due to the different atomic mass of dopants producing a different micro-strain on the vibrational modes inside the SCO complex [42]. The Raman spectra of SCO complex thin film on quartz substrate are essentially the same as that glass substrate [15,44]. All the available vibrational modes for stretching, bending, torsion etc. are depicted in Table 2.

The growth of the films on quartz surface and doping effects have also been monitored with optical absorption study at room temperature, as shown in Fig. 4. The absorption indicates that both the undoped and metal-doped (Zn, Mn) SCO thin films of $Fe(phen)_2(NCS)_2$ exhibit broad absorption peaks between 535 and 557 nm. These absorption peaks are the characteristic features of $^1A_{1g} \rightarrow {}^1T_{1g}$ ligand field absorption for the transition compound. This kind of feature is due to metal-ligand electron transmission from Fe d^6 orbital electron to π^* orbital of the phen-ligand for electromagnetic irradiation [15,37,38,47,48]. The obtained optical peak from absorption data for undoped and Zn/Mn-doped SCO thin-film complexes are given in Table 3 recorded at room temperature. The shift of optical absorption peaks in metal diluted SCO films plausibly occurred due to change in electronic configuration of Zn or Mn doped Fe $(phen)_2(NCS)_2$ lattice. The produced mechanical strain for the doped SCO thin films may also cause a possible change in the band structure [50,51].

The magnetic measurement is further used to confirm electronic spin states (HS↔LS) transition in undoped and metal-doped SCO thin film on quartz substrate by measuring the magnetization (M) vs. temperature (T) using SQUID magnetometer. This experiment has been carried with temperature variation between 100 and 300 K, and the magnetic field is kept constant at 1T. The temperature variation rate is held at 1 K min^{-1} for cooling and heating mode during this measurement. From experimentally obtained M-T data, the magnetic susceptibility (χ) of each of the three samples was further calculated. The computed susceptibilities

Table 1
Crystallographic information obtained from Rietveld analysis of XRD data.

Crystal information	Undoped Fe $(phen)_2(NCS)_2$ thin-film	Zn-doped Fe $(phen)_2(NCS)_2$ thin-film	Mn-doped Fe $(phen)_2(NCS)_2$ thin-film
Crystal System	Orthorhombic	Orthorhombic	Orthorhombic
Space Group	Pbcn	Pbcn	Pbcn
a (Å)	10.6255	10.5604	10.7920
b (Å)	10.0693	10.0129	10.1197
c (Å)	18.5161	18.1727	18.6765

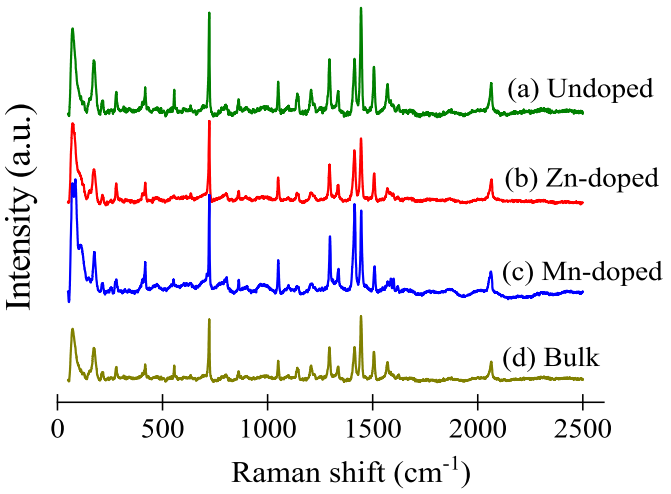

Fig. 3. Raman scattering spectra of (a) undoped, (b) Zn-doped, (c) Mn-doped spin-crossover thin films on quartz. The data has been compared with (d) bulk $Fe(phen)_2(NCS)_2$ at room temperature.

Table 2
Raman peaks for bulk, undoped and (Zn, Mn) doped thin films of spin-crossover complexes.

Details of Raman shift of SCO sample				Assignment
Bulk	Undoped thin film	Mn-doped (30%) thin film	Zn-doped (30%) thin film	Significance of modes
73	72	85	72	Symmetric FeN_6 torsion
173	173	175	174	Stretching and bending Fe–N
214	215	212	213	Symmetric Fe-N_{phen} stretching
418	418	418	417	Phen in-phase bending/out-phase C–C–C
723	723	722	722	Deformation heterocyclic ring
801	801	805	803	ν(NC–S)
862	862	863	863	(NC)–S asymmetric stretching
1050	1050	1051	1050	ν(C–C)
1141	1140	1145	1140	δ(C–H)
1207	1207	1206	1205	phen C–H in-plane bending
1295	1294	1296	1294	ν(C–N)
1336	1336	1338	1336	Phen ring stretching
1413	1413	1415	1412	In-plane C–H bending
1444	1444	1445	1445	Ring stretching
1506	1506	1510	1507	In-plane C–H bending
1572	1570	1586	1569	Ring stretching
2064	2064	2063	2065	SC-N symmetric stretching

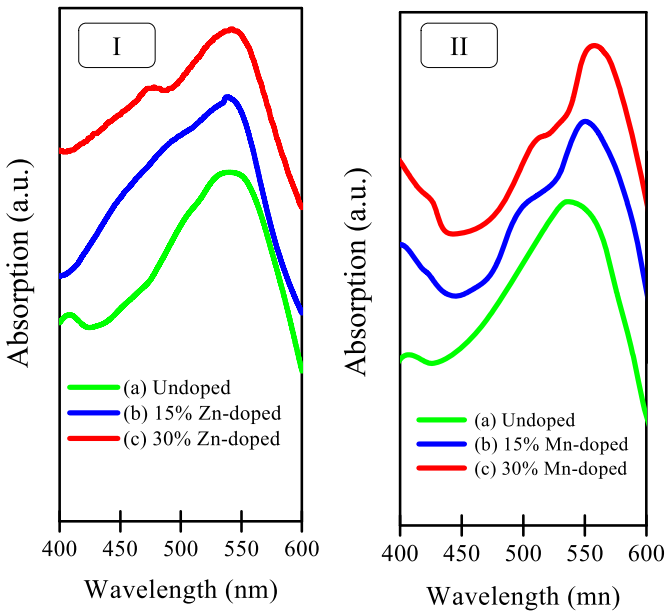

Fig. 4. Room temperature optical absorption spectra of (I) Zn-doped and (II) Mn-doped thin films of $Fe(phen)_2(NCS)_2$, respectively. The plotted curves are identified for (a) undoped (green curve), (b) 15% (blue curve), and (c) 30% (red curve) doped absorption spectra of SCO complexes. (For interpretation of the references to colour in this figure legend, the reader is referred to the web version of this article.)

Table 3
Obtained optical maximum absorption peak for undoped and metal (Zn or Mn) doped spin-crossover thin film of $Fe(phen)_2(NCS)_2$.

Sample	Undoped thin film	15% Metal-doped thin film	30% Metal-doped thin film
Zn-doped	535 nm	538 nm	543 nm
Mn-doped	535 nm	550 nm	557 nm

(χ) data is corrected for the constituent atoms' diamagnetism involving Pascal's constant [52]. For the undoped and doped SCO complexes, the χT may be estimated using the formula $\chi T = (1\text{-}x)\ \chi_{Fe}T + x\ \chi_{Zn/Mn}T$, where χ_{Fe} is the magnetic susceptibility of pure Fe and $\chi_{Zn/Mn}$ is the magnetic susceptibility of pure Zn/Mn [3]. The computed χT-T values, as illustrated in Fig. 5, are commonly used to describe the spin transition phenomena for each SCO samples.

The spin state transition is clearly revealed from the χT-T data as shown in Fig. 5 for the respective complexes. The representative data is provided here for undoped, metal (Zn or Mn) doped (30%) samples. The undoped SCO complex shows (Fig. 5a) an abrupt order spin transition with an evident hysteresis loop during its heating ↔ cooling modes. As the temperature rises, the net magnetization also changed, and the SCO complex goes through the spin state change LS↔HS. After achieving the HS state, the magnetization decreases with increasing temperature due to the polarity disturbance of SCO magnetic molecules. The magnetic response for the Zn-doped SCO thin-film shows similar spin transitions with a wider hysteresis loop (Fig. 5b). In contrast, the Mn-diluted thin film shows spin transition with a narrow hysteresis loop (Fig. 5c). The spin transition temperatures($T_{1/2}$) and loop widths of SCO thin film on quartz substrate are tabulated in Table 4 as inferred from Fig. 5 and compared with the results reported earlier on glass substrate [15].

The spin transition temperature($T_{1/2}$) shifts to the lower temperature region for metal-doped SCO thin film on the quartz shown in Fig. 5 [15,43,53]. A similar kind of behaviour is also retained in quartz as in the previous one. The possible reason for this kind of effect is the change in the internal pressure of the lattice during metal doping [54]. The ionic radii of Zn(II) (r = 76 pm) & Mn(II) (r = 81 pm) are nearly close to the Fe (II) (r = 78 p.m.) in the HS state, but in the LS state, the ionic radius of Fe (II) (r = 61 pm) is quite different from Zn and Mn ionic radii. The element used for doping with different ionic radii may develop a substantial strain inside the nanocrystal in the case of Zn or Mn substitution. This induced strain inside the SCO lattice generates 'negative' stress on the Fe(II) site, leads to an increase in the Fe–N bond distance (decrement in value of the crystal field potential), which favours the construction of host lattice stabilizing iron(II) HS state. So, metal dilution affects the usual energy level between HS and LS through the change in the molecular volume (ΔV_{HL}) and hence produced a negative pressure (p) during dilution [2,10,53,55,56]. The energy separation gap ΔE^0_{HL} within HS state and LS states for the undoped film is $\Delta E^0_{HL}(p) = \Delta E^0_{HL} - p\Delta V_{HL}$ and with temperature $\Delta E^0_{HL}(p) \propto k_B T$. It was reported that an approximate value for the bond length difference δ ~0.12 Å resulted from structural

Table 4
Comparisons of spin transition temperature ($T_{1/2}$) and hysteresis loop width for SCO samples on the quartz and the glass substrate. The data for glass substrate is taken from Ref. [15].

$Fe(phen)_2(NCS)_2$ thin film	$T_{1/2}$(K)↓ Quartz	$T_{1/2}$ (K)↓ Glass	$T_{1/2}$ (K)↑ Quartz	$T_{1/2}$ (K)↑ Glass	ΔT(K) Quartz	ΔT (K) Glass
(a) SCO undoped	167	170	183	180	16	10
(b) SCO Zn-doped	146	162	164	176	18	14
(c) SCO Mn-doped	155	149	160	158	5	9

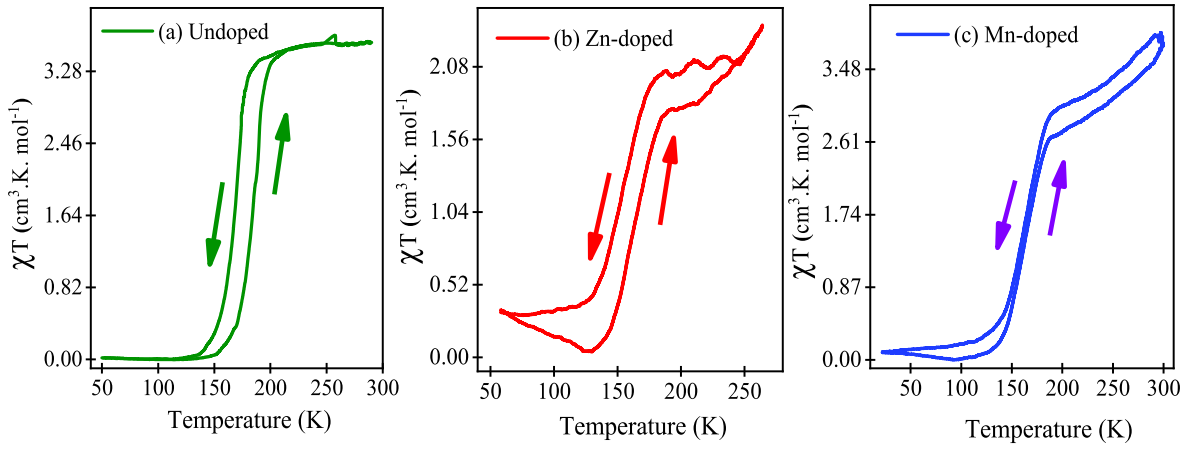

Fig. 5. χT vs. T plot of (a) undoped, (b) Zn-doped (30%) and (c) Mn-doped (30%) spin-crossover thin film during cooling ↔heating cycle.

study of $Fe(phen)_2(NCS)_2$ at high spin state (295 K) and low spin state (100 K) [57]. The spin state change induces modifications in volume of the whole material ΔV_{HL} ($(V_{HS}\text{-}V_{LS})/V_{LS}$). The volume change ~10–13% has been reported for various SCO complexes [58,59].

Hence a different amount of shift for transition temperature takes place for other metal diluted films. Also, the size of the nanocrystals and substrate specific growth of the molecular complex might have affected the transition temperatures ($T_{1/2}$) and the loop width, as shown in Table 4. The decrease in the nanoparticles' size leads to an effective increase in the metal's interaction and its surrounding ligand field causing an increase in the loop width. This different kind of magnetic response might have been influenced by the cooperativity between magnetic centres, the molecular environment of a substrate surface, crystal sizes, and periodic molecular uniformity on a microscopic level. The hysteresis loop width (ΔT) for the undoped SCO film is larger (16 K) on the quartz substrate than that of on glass substrate (10 K). Therefore, the results are quite significant in obtaining spin-state switching devices with the SCO nanocrystals to choose proper substrate and also doping with different metals. The nanocrystal size, dispersion, and the nanometric gap between them, and the choice of the substrate (and hence the film growth) are the factors to tune the spin state switching with a wider hysteresis loop and transition temperatures. The hysteretic behaviour obtained from magnetic data for both doped and undoped spin-crossover thin films of $Fe(phen)_2(NCS)_2$ and the different substrate surface is crucial for using spin-crossover films to fabricate spin-state switching memory devices.

4. Conclusions

In conclusion, we have described here a method to obtain a spin-crossover molecular thin film of $Fe(phen)_2(NCS)_2$ on a quartz substrate, which is quite essential for the fabrication of spin-based devices. Further, we also obtained metal (Zn or Mn) doped SCO films to alter the magnetic responses of the molecules. The films thus obtained were characterized by XRD, SEM, and Raman studies. For clarity, we compared the results thus obtained for both quartz and glass substrates. Indeed, spin-state switching is found to be critically dependent on molecular growth on the substrate and possibly doping effects. The hysteresis loop obtained in calculated magnetic susceptibility results provides information on spin-state transition temperature and loop width. The study shows that metal doping results a shift of transition temperature during HS↔LS electronic transitions. It can be interpreted as the strain developed during the insertion of metal in the SCO lattice, creating negative pressure inside the host complex. The results presented here therefore may be fruitful for designing spin-state-based devices in future.

Credit author statement

All the authors contributed equally to the manuscript.

Declaration of competing interest

The authors declare that they have no known competing financial interests or personal relationships that could have appeared to influence the work reported in this paper.

Data availability

No data was used for the research described in the article.

Acknowledgments

CSIR, Govt. of India is acknowledged with thanks for providing SRF to Saroj Saha. The CSR-UGC DAE Indore and Kolkata centres are also acknowledged with thanks for providing the XRD and SQUID measurement facilities.

References

[1] A. Bousseksou, G. Molnár, P. Demont, J. Menegotto, Observation of a thermal hysteresis loop in the dielectric constant of spin crossover complexes: towards molecular memory devices, J. Mater. Chem. 13 (2003) 2069–2071, https://doi.org/10.1039/b306638j.
[2] C. Baldé, C. Desplanches, J. François Létard, G. Chastanet, Effects of metal dilution on the spin-crossover behavior and light induced bistability of iron(II) in [FexNi1−x(bpp)2](NCSe)2, Polyhedron 123 (2017) 138–144, https://doi.org/10.1016/j.poly.2016.08.046.
[3] T. Tayagaki, A. Galet, G. Molnár, M. Carmen Muñoz, A. Zwick, K. Tanaka, J. A. Real, A. Bousseksou, Metal dilution effects on the spin-crossover properties of the three-dimensional coordination polymer Fe(pyrazine)[Pt(CN) 4], J. Phys. Chem. B 109 (2005) 14859–14867, https://doi.org/10.1021/jp0521611.
[4] H.S. Scott, T.M. Ross, N.F. Chilton, I.A. Gass, B. Moubaraki, G. Chastanet, N. Paradis, J.F. Lètard, K.R. Vignesh, G. Rajaraman, S.R. Batten, K.S. Murray, Crown-linked dipyridylamino-triazine ligands and their spin-crossover iron(ii) derivatives: magnetism, photomagnetism and cooperativity, Dalton Trans. 42 (2013) 16494–16509, https://doi.org/10.1039/c3dt51839f.
[5] P. Gütlich, Y. Garcia, H.A. Goodwin, Spin crossover phenomena in Fe(II) complexes, Chem. Soc. Rev. 29 (2000) 419–427, https://doi.org/10.1039/b003504l.
[6] W.A. Baker, H.M. Bobonich, Magnetic properties of some high-spin complexes of iron(II), Inorg. Chem. 3 (1964) 1184–1188, https://doi.org/10.1021/ic50018a027.
[7] P. Gütlich, V. Ksenofontov, A.B. Gaspar, Pressure effect studies on spin crossover systems, Coord. Chem. Rev. 249 (2005) 1811–1829, https://doi.org/10.1016/j.ccr.2005.01.022.
[8] A. Bousseksou, N. Negre, M. Goiran, L. Salmon, J.P. Tuchagues, M.L. Boillot, K. Boukheddaden, F. Varret, Dynamic triggering of a spin-transition by a pulsed magnetic field, Eur. Phys. J. B 13 (2000) 451–456, https://doi.org/10.1007/s100510050057.
[9] G. Molnár, V. Niel, J.A. Real, L. Dubrovinsky, A. Bousseksou, J.J. McGarvey, Raman spectroscopic study of pressure effects on the spin-crossover coordination polymers Fe(pyrazine)[M(CN)4]·2H2O (M = Ni, Pd, Pt). First observation of a piezo-hysteresis loop at room temperature, J. Phys. Chem. B 107 (2003) 3149–3155, https://doi.org/10.1021/jp027550z.
[10] A. Hauser, Light-induced spin crossover and the high-Spin→Low-spin relaxation, in: Springer, Springer, Berlin, Heidelberg, 2012, pp. 155–198, https://doi.org/10.1007/b95416.
[11] S. Cobo, D. Ostrovskii, S. Bonhommeau, L. Vendier, G. Molnár, L. Salmon, K. Tanaka, A. Bousseksou, Single-laser-shot-induced complete bidirectional spin transition at room temperature in single crystals of (FeII(pyrazine)(Pt(CN) 4)), J. Am. Chem. Soc. 130 (2008) 9019–9024, https://doi.org/10.1021/ja800878f.
[12] S. De, L.M. Chamoreau, H. El Said, Y. Li, A. Flambard, M.L. Boillot, S. Tewary, G. Rajaraman, R. Lescouëzec, Thermally-induced spin crossover and LIESST effect in the neutral [FeII(Mebik)2(NCX)2] complexes: variable-temperature structural, magnetic, and optical studies (X = S, Se; Mebik = bis(1-methylimidazol-2-yl) ketone), Front. Chem. 6 (2018), https://doi.org/10.3389/fchem.2018.00326.
[13] M. Quesada, M. Monrabal, G. Aromí, V.A. De La Peña-O'Shea, M. Gich, E. Molins, O. Roubeau, S.J. Teat, E.J. MacLean, P. Gamez, J. Reedijk, Spin transition in a triazine-based Fe(ii) complex: variable-temperature structural, thermal, magnetic and spectroscopic studies, J. Mater. Chem. 16 (2006) 2669–2676, https://doi.org/10.1039/b602903e.
[14] P.O. Ribeiro, B.P. Alho, R.M. Ribas, E.P. Nóbrega, V.S.R. de Sousa, P.J. von Ranke, Influence of magnetic field on a spin-crossover material, J. Magn. Magn Mater. 489 (2019), https://doi.org/10.1016/j.jmmm.2019.165340.
[15] S. Saha, S.K. Mandal, Spin transition properties of metal (Zn, Mn) diluted Fe(phen) 2(NCS)2spin-crossover thin films, EPJ Appl. Phys. 91 (2020), 20301, https://doi.org/10.1051/epjap/2020200056.
[16] A. Desaix, O. Roubeau, J. Jeftic, J.G. Haasnoot, K. Boukheddaden, E. Codjovi, J. Linarès, M. Noguès, F. Varret, Light-induced bistability in spin transition solids leading to thermal and optical hysteresis, Eur. Phys. J. B 6 (1998) 183–193, https://doi.org/10.1007/s100510050540.
[17] L. Salmon, L. Catala, Spin-crossover nanoparticles and nanocomposite materials, Compt. Rendus Chem. 21 (2018) 1230–1269, https://doi.org/10.1016/j.crci.2018.07.009.
[18] P. Ganguli, P. Gütlich, E.W. Müller, Effect of metal dilution on the spin-crossover behavior in [FexM1−x(phen)2(NCS)2] (M = Mn, Co, Ni, Zn), Inorg. Chem. 21 (1982) 3429–3433, https://doi.org/10.1021/ic00139a032.
[19] B. Gallois, C. Hauw, J.A. Real, J. Zarembowitch, Structural changes associated with the spin transition in Fe(phen)2(NCS)2: a single-crystal X-ray investigation, Inorg. Chem. 29 (1990) 1152–1158, https://doi.org/10.1021/ic00331a009.
[20] P. Gütlich, A. Hauser, H. Spiering, Thermal and optical switching of iron(II) complexes, Angew. Chem. Int. Ed. Engl. 33 (1994) 2024–2054, https://doi.org/10.1002/anie.199420241.
[21] M. Cavallini, I. Bergenti, S. Milita, G. Ruani, I. Salitros, Z.R. Qu, R. Chandrasekar, M. Ruben, Micro- and nanopatterning of spin-transition compounds into logical structures, Angew. Chem. Int. Ed. 47 (2008) 8596–8600, https://doi.org/10.1002/anie.200802085.
[22] O. Kahn, C.J. Martinez, Spin-transition polymers: from molecular materials toward memory devices, Science 80 (279) (1998) 44–48, https://doi.org/10.1126/science.279.5347.44.

[23] J. Linares, E. Codjovi, Y. Garcia, Pressure and temperature spin crossover sensors with optical detection, Sensors 12 (2012) 4479–4492, https://doi.org/10.3390/s120404479.
[24] P.J. von Ranke, B.P. Alho, E.P. Nobrega, A. Caldas, V.S.R. de Sousa, M.V. Colaço, L. F. Marques, G.M. Rocha, D.L. Rocco, P.O. Ribeiro, The refrigerant capacity in spin-crossover materials: application to [Fe(phen)2(NCS)2], J. Magn. Magn Mater. 489 (2019), https://doi.org/10.1016/j.jmmm.2019.165421.
[25] H.S. Abdelkader, B. Berrahil, G. Merad, Effect of Ca doping on structural, magnetic and electronic properties of TbMnO 3, J. Magn. Magn. Mater. 477 (2019) 77–82, https://doi.org/10.1016/j.jmmm.2019.01.022.
[26] D. Chakraborty, K. Shaik, Effect of doping concentration, temperature and magnetic field on magnetic properties of Mn doped ITO nanoparticles and thin films, J. Magn. Magn. Mater. 486 (2019), https://doi.org/10.1016/j.jmmm.2019.165268.
[27] Z. Ni, X. Guo, Q. Li, Z. Liang, H. Luo, F. Meng, Effect of Zn-doping on the phase transition and magnetic properties of Heusler alloys Ni2MnGa1−xZnx (x = 0, 0.25, 0.5, 0.75 and 1), J. Magn. Magn. Mater. 464 (2018) 65–70, https://doi.org/10.1016/j.jmmm.2018.05.044.
[28] Y.J. Tang, Transition-metal substitution effect on magnetic and magnetostrictive properties of TbFe2 compounds, J. Magn. Magn. Mater. 167 (1997) 245–248, https://doi.org/10.1016/S0304-8853(96)00331-9.
[29] P. Shunmuga Sundaram, G. Arivazhagan, S.S.R. Inbanathan, S. Hussian, E. Manikandan, A. Umar, M. Ajmal Khan, H. Algarni, Structural, optical and magnetic properties of Zn 1- x Co x O nanoparticles, J. Nanosci. Nanotechnol. 20 (2020) 5525–5532, https://doi.org/10.1166/jnn.2020.17812.
[30] M.G. Song, J.Y. Han, C.W. Bark, Effects of doping ratio of cobalt and iron on the structure and optical properties of Bi3.25La0.75FexCo1-xTi2O12 (X = 0, 0.25, 0.5, 0.75, 1), J. Nanosci. Nanotechnol. 15 (2015) 7841–7844, https://doi.org/10.1166/jnn.2015.11183.
[31] D. Qiu, J. Wu, L. Liang, H. Zhang, H. Cao, W. Yong, T. Tian, J. Gao, F. Zhuge, Structural and electrochromic properties of undoped and Mo-doped V 2 O 5 thin films by a two-electrode electrodeposition, J. Nanosci. Nanotechnol. 18 (2018) 7502–7507, https://doi.org/10.1166/jnn.2018.16067.
[32] Y. Vygranenko, M. Fernandes, M. Vieira, G. Lavareda, C. Nunes De Carvalho, P. Brogueira, A. Amaral, Photoconductivity kinetics of indium sulfofluoride thin films, EPJ Appl. Phys. 89 (2020), https://doi.org/10.1051/epjap/2020190265.
[33] J.P. Kleider, E. Johnson, R. Brüggemann, A. Torres, M. Moreno, P. Rosales, M. Dominguez, A. Torres, A. Morales, A. Itzmoyotl, J. De La Hidalga, Study of nanocrystalline silicon-germanium for the development of thin film transistors, EPJ Appl. Phys. 89 (2020), 10102, https://doi.org/10.1051/epjap/2020190264.
[34] V. Şenay, S. Özen, Some physical properties of a Li 4 Ti 5 O 12 thin film electrode manufactured by radio frequency magnetron sputtering, Eur. Phys. J. Appl. Phys. 87 (2019), 10302, https://doi.org/10.1051/epjap/2019190007.
[35] S. Shanmugan, D. Mutharasu, Z.Y. Lee, Surface and electrical properties of plasma processed RF sputtered GaN thin films, EPJ Appl. Phys. 68 (2014), https://doi.org/10.1051/epjap/2014140225.
[36] G. Wang, X. Zhang, W. Jiang, L. Wang, A study on the structure and the photoelectrical properties of the Al-doped ZnO thin films by atomic layer deposition in low temperatures, J. Nanosci. Nanotechnol. 18 (2018) 8333–8336, https://doi.org/10.1166/jnn.2018.16378.
[37] C. Mondal, S.K. Mandal, Electrically controllable molecular spin crossover switching in Fe(phen)2(NCS)2 thin film, EPJ Appl. Phys. 75 (2016), https://doi.org/10.1051/epjap/2016160258.
[38] C. Mondal, S. Pal, S.K. Mandal, Probing spin-state switching in Fe(phen) 2 (NCS) 2 thin film nanocrystals on different substrates by electrical conductivity measurements, J. Nanosci. Nanotechnol. 18 (2017) 347–352, https://doi.org/10.1166/jnn.2018.14602.
[39] S. Brooker, Spin crossover with thermal hysteresis: practicalities and lessons learnt, Chem. Soc. Rev. 44 (2015) 2880–2892, https://doi.org/10.1039/C4CS00376D.
[40] K. Akabori, H. Matsuo, Y. Yamamoto, Thermal properties of tris(1,10-phenanthroline) complexes of iron(II) and nickel(II) salts, J. Inorg. Nucl. Chem. 35 (1973) 2679–2690, https://doi.org/10.1016/0022-1902(73)80498-1.
[41] N. Tsuchiya, T. Isobe, M. Senna, N. Yoshioka, H. Inoue, Mechanochemical effects on the structures and chemical states of [Fe(Phen)3](NCS)2·H2O, Solid State Commun. 99 (1996) 525–529, https://doi.org/10.1016/0038-1098(96)00359-6.
[42] D.P. Dutta, P. Raval, Effect of transition metal ion (Cr3+, Mn2+ and Cu2+) doping on the photocatalytic properties of ZnWO4 nanoparticles, J. Photochem. Photobiol. Chem. 357 (2018) 193–200, https://doi.org/10.1016/j.jphotochem.2018.02.026.
[43] C. Lefter, S. Tricard, H. Peng, G. Molnár, L. Salmon, P. Demont, A. Rotaru, A. Bousseksou, Metal substitution effects on the charge transport and spin crossover properties of [Fe1- xZnx(Htrz)2(trz)](BF4) (trz = Triazole), J. Phys. Chem. C 119 (2015) 8522–8529, https://doi.org/10.1021/acs.jpcc.5b01117.
[44] C. Mondal, M.L. Nanda Goswami, S.K. Mandal, Frequency dependent charge transport and spin state switching characteristics of Fe(phen) 2 (NCS) 2 in polymer, J. Nanosci. Nanotechnol. 20 (2019) 2803–2812, https://doi.org/10.1166/jnn.2020.17444.
[45] E. Konig, K. Madeja, 5T2-1A1 Equilibriums in some iron(II)-bis(1,10-phenanthroline) complexes, Inorg. Chem. 6 (1967) 48–55, https://doi.org/10.1021/ic50047a011.
[46] A. Bousseksou, J.J. McGarvey, F. Varret, J.A. Real, J.P. Tuchagues, A.C. Dennis, M. L. Boillot, Raman spectroscopy of the high- and low-spin states of the spin crossover complex Fe(phen)2(NCS)2: an initial approach to estimation of vibrational contributions to the associated entropy changeDedication to Professor Olivier Kahn, we are very sad that yo, Chem. Phys. Lett. 318 (2000) 409–416, https://doi.org/10.1016/S0009-2614(00)00063-4.
[47] E. Collet, G. Azzolina, T. Ichii, L. Guerin, R. Bertoni, A. Moréac, M. Cammarata, N. Daro, G. Chastanet, J. Kubicki, K. Tanaka, S.F. Matar, Lattice phonon modes of the spin crossover crystal [Fe(phen) 2 (NCS) 2] studied by THz, IR, Raman spectroscopies and DFT calculations, Eur. Phys. J. B 92 (2019) 12, https://doi.org/10.1140/epjb/e2018-90553-2.
[48] J.P. Jesson, S. Trofimenko, D.R. Eaton, Spin equilibria in octahedral iron(II) poly (1-pyrazolyl) borates, J. Am. Chem. Soc. 89 (1967) 3158–3164, https://doi.org/10.1021/ja00989a015.
[50] A. Vazinishayan, S. Yang, D.R. Lambada, G. Zhang, Y. Wang, Investigation of the effects of tensile strain on optical properties of ZnO nanowire, Chin. J. Phys. 56 (2018) 1799–1809, https://doi.org/10.1016/j.cjph.2018.07.017.
[51] Y. Liang, S. Huang, L. Yang, Many-electron effects on optical absorption spectra of strained graphene, J. Mater. Res. 27 (2012) 403–409, https://doi.org/10.1557/jmr.2011.412.
[52] G.A. Bain, J.F. Berry, Diamagnetic corrections and Pascal's constants, J. Chem. Educ. 85 (2008) 532–536, https://doi.org/10.1021/ED085P532.
[53] C. Baldé, C. Desplanches, F. Le Gac, P. Guionneau, J.F. Létard, The role of iron(ii) dilution in the magnetic and photomagnetic properties of the series [FexZn1-x (bpp)2](NCSe) 2, Dalton Trans. 43 (2014) 7820–7829, https://doi.org/10.1039/c3dt52964a.
[54] H. Wang, C. Baldé, A. Grosjean, C. Desplanches, P. Guionneau, G. Chastanet, Seven-coordinated iron(ii) spin-crossover molecules: some learning from iron substitution in [Fe: XMn1- x(L222N3O2)(CN)2]·H2O solid solutions, Dalton Trans. 47 (2018) 14741–14750, https://doi.org/10.1039/c8dt02517g.
[55] S. Iwai, S. Nakashima, Spin-crossover phenomenon and intermolecular interaction for the assembled Fe(II) complexes having aromatic rings, Hyperfine Interact. 241 (2020) 54, https://doi.org/10.1007/s10751-020-01719-x.
[56] P. Gütlich, A.B. Gaspar, Y. Garcia, V. Ksenofontov, Pressure effect studies in molecular magnetism, Compt. Rendus Chem. 10 (2007) 21–36, https://doi.org/10.1016/j.crci.2006.09.011.
[57] E. König, K.J. Watson, The Fe–N bond lengths, the "ionic radii" of iron (II), and the crystal field parameters (10Dq) in a high-spin and low-spin [FeII-N6] complex, Chem. Phys. Lett. 6 (1970) 457–459, https://doi.org/10.1016/0009-2614(70)85191-0.
[58] E. Collet, P. Guionneau, Structural analysis of spin-crossover materials: from molecules to materials, Compt. Rendus Chem. 21 (2018) 1133–1151, https://doi.org/10.1016/J.CRCI.2018.02.003.
[59] P. Guionneau, Crystallography and spin-crossover. A view of breathing materials, Dalton Trans. 43 (2013) 382–393, https://doi.org/10.1039/C3DT52520A.